AIAA JOURNAL
Vol. 52, No. 11, November 2014

Composite Interaction Energy and Constituent Average Stresses for Predicting Composite Failure

Kedar A. Malusare* and Ray S. Fertig III†
University of Wyoming, Laramie, Wyoming 82071

DOI: 10.2514/1.J052890

Complex interactions in fiber-reinforced composites between multiple failure mechanisms have made accurate failure prediction a daunting challenge. One approach to better identify failure mechanisms has been the use of volume average constituent stresses in the composite to predict the onset and outcome of failure in individual constituents. However, this approach was shown here to not conserve strain energy in the composite, which could potentially affect the accuracy of failure prediction under certain loading conditions. The focus of this work was to develop an expression for the discrepancy in strain energy, termed the interaction energy, and to numerically evaluate the influence of constituent properties, fiber volume fraction, and load combinations on the magnitude of this energy. The simulation results showed that interaction energy accounts for nearly 30% of the total strain energy in the composite for certain loading conditions in typical aerospace-grade carbon-epoxy composites, suggesting that existing constituent-based failure theories might be enhanced by incorporation of this energy into failure criteria.

Nomenclature

U	=	total composite strain energy
U_f	=	fiber strain energy
U_m	=	matrix strain energy
V_c	=	composite volume
V_f	=	total fiber volume
V_m	=	total matrix volume
ε	=	local strain
$\tilde{\varepsilon}$	=	local fluctuation in strain
$\langle\varepsilon\rangle$	=	mean strain
ε^C	=	composite strain
ε^f	=	strain induced in the fiber
ε^m	=	strain in the matrix constituent
σ^C	=	composite stress
σ^f	=	stress induced in the fiber
σ^m	=	stress in the matrix constituent
Φ_f	=	fiber interaction energy density
Φ_m	=	matrix interaction energy density

I. Introduction

THE use of composite materials in the wind and aerospace industries has grown dramatically in recent years, with composites comprising 50% or more of The Boeing Company's 787 and Airbus SAS's A350. With this increase in use has come a greater demand for design tools that can accurately predict damage initiation and propagation, durability, and remaining life. This has proven to be quite challenging due the range of complex failure behaviors exhibited by composites. Unlike conventional homogeneous materials like metals, the constituent undergoing failure may switch rapidly, and the failure mechanisms within each constituent can vary widely depending on the loading. At the lamina level, tensile loads parallel to the fiber direction may cause both fiber and matrix fracture. Under transverse loading, mode I matrix cracking or fiber/matrix debonding may occur in tension, with a shear matrix failure occurring in compression. At the laminate level, delamination may occur, which will substantially affect the distribution of stresses in each lamina. This complexity has resulted in a large number of proposed composite failure theories with no clearly superior choice.

The First and Second World-Wide Failure Exercises (WWFE I and WWFE II, respectively) have provided a much needed benchmark against which to compare the effectiveness of various composite failure theories for both glass- and carbon-fiber composites over complex loading configurations [1–3]. One distinction among failure theories was the use of micromechanics in the prediction of failure, such that various measures of fiber and matrix constituent stresses were used to predict lamina failure rather than using lamina-level failure criteria to predict failure. These included microstress theory [4,5], micromechanics of failure [6,7], multicontinuum theory [8–10], and a bridging model that combines micromechanics with anisotropic plasticity [11–13]. In addition to the theories used in WWFE I or II, other well-known constituent-based composite failure theories are commonly used, such as the generalized method of cells [14–20] and strain invariant failure theory [21,22]. Although none of the previous theories were judged in the benchmark exercises to exceed the performance of more established theories, they were assessed as evolving toward maturity [3]. But the unique appeal of constituent-level failure theories is not simply in static failure prediction, but their potential for physics-based modeling and materials design efforts, such as the Materials Genome Initiative [23] and Integrated Computational Materials Engineering [24].

The methods used to extract constituent stresses and strains from composite stresses typically use some form of a localization tensor to map composite stresses to constituent stresses, which may be evaluated at specific points or as volume average quantities. The use of constituent stresses at specific points is strongly dependent on the choice of representative volume element (RVE) for the composite microstructure. Any deviation from the idealized structure may substantially alter the stress at a particular location. The use of volume average stresses is appealing because it is less sensitive to details of the microstructure; random fiber packing and idealized hexagonal fiber packing will yield nearly the same average constituent stresses and strains. However, the use of volume average constituent stresses and strains may not account for the total strain energy in a composite. For example, a careful inspection of the stress fields in a composite microstructure reveals the presence of shear stresses in the constituents, even when the composite loading is purely transverse normal; these stresses, however, average to zero and therefore cannot be accounted for in any failure or material nonlinearity model. As a result, failure prediction under particular

Presented as Paper 2013-1723 at the 54th AIAA/ASME/ASCE/AHS/ASC Structures, Structural Dynamics, and Materials Conference, Boston, MA, 8–11 April 2013; received 21 June 2013; revision received 10 March 2014; accepted for publication 11 March 2014; published online 18 June 2014.

*Graduate Student, Department of Mechanical Engineering, Dept. 3295. Student Member AIAA.

†Assistant Professor, Department of Mechanical Engineering, Dept. 3295. Member AIAA.

loading configurations may not be consistent with bulk constituent properties because a significant portion of the strain energy may be unaccounted for. The energy not accounted for when using volume average constituent stresses and strains is termed the interaction energy.

To enhance physics-based composite failure prediction, all strain energy should be accounted for. The goal of this paper is to provide a quantitative foundation for the development of constituent-level composite failure theories based on the conservation of strain energy across length scales. As such, the focus of this research is to quantify the magnitude of the interaction energy relative to the total strain energy for a variety of fiber volume fractions, matrix elastic properties, and complex multi-axial loading configurations. The reported results clearly indicate that a significant fraction of energy is unaccounted for under a variety of loading conditions in typical aerospace composite materials but also suggest that this interaction energy could be readily incorporated into constituent failure criteria.

II. Theoretical Motivation

This section focuses on establishing the equations that can be used to quantify the interaction energy. Consider an RVE of a composite material consisting of fiber and matrix phases. Let U denote the strain energy of this composite under an arbitrary load state. Assuming a linear elastic material, this energy can be represented as

$$U = \frac{1}{2}\int_{V_C} \sigma_{ij}^C \varepsilon_{ij}^C \, \mathrm{d}V_C \tag{1}$$

where σ_{ij}^C and ε_{ij}^C are the composite stresses and strains, respectively; repeated ij indices are summed, and integration is performed over the entire volume of the composite V_c. For a periodic RVE subject to homogeneous boundary conditions as defined by Hashin [25], Eq. (1) can be readily written in terms of average composite properties [26–28]:

$$U = \frac{1}{2}\langle\sigma_{ij}^C\rangle\langle\varepsilon_{ij}^C\rangle V_C \tag{2}$$

where the terms in the brackets denote volume average quantities. Strain energy may be separated into contributions from the fiber and the matrix:

$$U = U_f + U_m \tag{3}$$

such that

$$U_f = \frac{1}{2}\int_{V_f} \sigma_{ij}^f \varepsilon_{ij}^f \, \mathrm{d}V_f \tag{4}$$

$$U_m = \frac{1}{2}\int_{V_m} \sigma_{ij}^m \varepsilon_{ij}^m \, \mathrm{d}V_m \tag{5}$$

where the superscripts f and m denote quantities for fiber and matrix, respectively. In contrast to using average lamina stresses, summing the strain energies of the constituents computed using constituent volume average stresses does not account for all of the strain energy in the composite. The energy that is unaccounted for is termed the interaction energy. To quantify this energy, the strains in each constituent are written in terms of a mean value $\langle\varepsilon_{ij}\rangle$ plus a fluctuation $\tilde{\varepsilon}_{ij}$; similarly, the stresses are also written as a mean value $\langle\sigma_{ij}\rangle$ plus a fluctuation $\tilde{\sigma}_{ij}$:

$$\varepsilon_{ij} = \tilde{\varepsilon}_{ij} + \langle\varepsilon_{ij}\rangle \tag{6}$$

$$\sigma_{ij} = \tilde{\sigma}_{ij} + \langle\tilde{\sigma}_{ij}\rangle \tag{7}$$

For the fiber, Eqs. (6) and (7) are substituted into Eq. (4) to obtain

$$U_f = \frac{1}{2}\int_{V_f} ((\langle\sigma_{ij}^f\rangle + \langle\tilde{\sigma}_{ij}^f\rangle)(\langle\varepsilon_{ij}^f\rangle + \langle\tilde{\varepsilon}_{ij}^f\rangle)) \, \mathrm{d}V_f \tag{8}$$

Expanding Eq. (8) yields

$$U_f = \frac{1}{2}\int_{V_f} \langle\sigma_{ij}^f\rangle\langle\varepsilon_{ij}^f\rangle \, \mathrm{d}V_f + \frac{1}{2}\int_{V_f} \tilde{\sigma}_{ij}^f\tilde{\varepsilon}_{ij}^f \, \mathrm{d}V_f + \frac{1}{2}\int_{V_f} \langle\sigma_{ij}^f\rangle\tilde{\varepsilon}_{ij}^f \, \mathrm{d}V_f + \frac{1}{2}\int_{V_f} \tilde{\sigma}_{ij}^f\langle\varepsilon_{ij}^f\rangle \, \mathrm{d}V_f \tag{9}$$

which, on further simplification, gives

$$U_f = \frac{1}{2}\langle\sigma_{ij}^f\rangle\langle\varepsilon_{ij}^f\rangle V_f + \frac{1}{2}\int_{V_f} \tilde{\sigma}_{ij}^f\tilde{\varepsilon}_{ij}^f \, \mathrm{d}V_f \tag{10}$$

because volume average quantities are constant, and $\tilde{\sigma}_{ij}^f$ and $\tilde{\varepsilon}_{ij}^f$ are local fluctuations with averages that are identically zero. The matrix contribution is derived in a similar manner to give

$$U_m = \frac{1}{2}\langle\sigma_{ij}^m\rangle\langle\varepsilon_{ij}^m\rangle V_m + \frac{1}{2}\int_{V_m} \tilde{\sigma}_{ij}^m\tilde{\varepsilon}_{ij}^m \, \mathrm{d}V_m \tag{11}$$

The strain energies in the fiber and matrix can then be written as

$$U_f = \frac{1}{2}\langle\sigma_{ij}^f\rangle\langle\varepsilon_{ij}^f\rangle V_f + \Phi_f V_f \tag{12}$$

$$U_m = \frac{1}{2}\langle\sigma_{ij}^m\rangle\langle\varepsilon_{ij}^m\rangle V_m + \Phi_m V_m \tag{13}$$

where Φ_f and Φ_m are the fiber and matrix contributions to the interaction energy density, respectively given by

$$\Phi_f = \frac{1}{2V_f}\int_{V_f} \tilde{\sigma}_{ij}^f\tilde{\varepsilon}_{ij}^f \, \mathrm{d}V_f \tag{14}$$

$$\Phi_m = \frac{1}{2V_m}\int_{V_m} \tilde{\sigma}_{ij}^m\tilde{\varepsilon}_{ij}^m \, \mathrm{d}V_m \tag{15}$$

The interaction energy ΔU is thus related to the total strain energy and the energy computed from volume average constituent quantities via

$$U = U_m + U_f = \frac{1}{2}\langle\sigma_{ij}^m\rangle\langle\varepsilon_{ij}^m\rangle V_m + \frac{1}{2}\langle\sigma_{ij}^f\rangle\langle\varepsilon_{ij}^f\rangle V_f + \Delta U \tag{16}$$

where

$$\Delta U = \Phi_f V_f + \Phi_m V_m \tag{17}$$

Substituting Hooke's law into Eq. (14) allows the interaction energy density to be written entirely in terms of strain fluctuations:

$$\Phi_f = \frac{1}{2V_f}\int_{V_f} C_{ijkl}\tilde{\varepsilon}_{ij}^f\tilde{\varepsilon}_{kl}^f \, \mathrm{d}V_f = \frac{1}{2V_f}\int_{V_f} C_{mn}^f\tilde{\varepsilon}_m^f\tilde{\varepsilon}_n^f \, \mathrm{d}V_f \tag{18}$$

where C^f_{mn} is the m, n component of the 6×6 fiber stiffness matrix. Assuming transverse isotropy and expanding Eq. (18) yields

$$2\Phi_f = C^f_{11}\langle(\tilde{\varepsilon}^f_{11})^2\rangle + C^f_{22}\langle(\tilde{\varepsilon}^f_{22})^2\rangle + C^f_{33}\langle(\tilde{\varepsilon}^f_{33})^2\rangle + 2C^f_{12}\langle\tilde{\varepsilon}^f_{11}\cdot\tilde{\varepsilon}^f_{22}\rangle + 2C^f_{12}\langle\tilde{\varepsilon}^f_{11}\cdot\tilde{\varepsilon}^f_{33}\rangle + 2C^f_{23}\langle\tilde{\varepsilon}^f_{22}\cdot\tilde{\varepsilon}^f_{33}\rangle + C^f_{44}\langle(\tilde{\gamma}^f_{12})^2\rangle + C^f_{44}\langle(\tilde{\gamma}^f_{13})^2\rangle + C^f_{66}\langle(\tilde{\gamma}^f_{23})^2\rangle \quad (19)$$

The interaction energy density for the matrix can be similarly shown to be

$$2\Phi_m = C^m_{11}\langle(\tilde{\varepsilon}^m_{11})^2\rangle + C^m_{22}\langle(\tilde{\varepsilon}^m_{22})^2\rangle + C^m_{33}\langle(\tilde{\varepsilon}^m_{33})^2\rangle + 2C^m_{12}\langle\tilde{\varepsilon}^m_{11}\cdot\tilde{\varepsilon}^m_{22}\rangle + 2C^m_{12}\langle\tilde{\varepsilon}^m_{11}\cdot\tilde{\varepsilon}^m_{33}\rangle + 2C^m_{23}\langle\tilde{\varepsilon}^m_{22}\cdot\tilde{\varepsilon}^m_{33}\rangle + C^m_{44}\langle(\tilde{\gamma}^m_{12})^2\rangle + C^m_{44}\langle(\tilde{\gamma}^m_{13})^2\rangle + C^m_{66}\langle(\tilde{\gamma}^m_{23})^2\rangle \quad (20)$$

Equations (19) and (20) quantify the interaction energy between fiber and matrix, but they contain a total of 18 terms. The focus of the subsequent modeling effort is to determine the significance of the interaction energy relative to the total strain energy, to investigate how the interaction energy may change as a function of loading and material properties, and to attempt to establish relative contribution of each constituent to the interaction energy.

III. Finite-Element Modeling

A finite-element model was developed and studied using Abaqus [29] to investigate the magnitude of the interaction energy as a function of fiber volume fraction, elastic moduli of the constituents, and varying loading conditions. For the purpose of analysis, a representative volume element (RVE) of a hexagonal fiber packing was modeled, as shown in Fig. 1, where fiber cross sections are darkly shaded, and the remainder is matrix material. Periodic boundary conditions were applied on all RVE edges, faces, and corners. This was achieved by extracting nodes from the RVE after meshing, reordering them properly, and using equation constraints for the node sets. The axial direction of the fibers is defined as the 1-direction (longitudinal). Carbon fiber properties (AS4) reported by Sun and Vaidya [26] and shown in Table 1 were used for all simulations. The matrix was assumed to be isotropic with a Poisson's ratio of 0.34.

Three parametric studies were conducted. First, the fiber volume fraction was varied from 0.05 to 0.85, with the matrix modulus fixed at 1% of the fiber-direction fiber modulus $E_m = 2.35$ GPa. In the second study, the matrix modulus was varied from 1 to 120% of the fiber modulus in the fiber direction. (A matrix modulus of $0.0204 \times E_{11\text{fiber}}$ roughly corresponds to epoxy 3501-6; $E_m = 4.8$ GPa.) Results for the modulus study were obtained for four different fiber volume fractions of 0.05, 0.25, 0.6, and 0.85. In both of these parametric studies, four unique composite loading states were examined: $\varepsilon_{11}, \varepsilon_{22}, \varepsilon_{12}$, and ε_{23}. These loads were achieved by fixing displacements of the RVE control nodes such that a strain of 0.01 was applied in each load case, with all other strains held fixed at zero. In the third study, five types of biaxial loads were applied: $\sigma_{22} - \sigma_{33}$, $\sigma_{12} - \sigma_{22}$, $\sigma_{12} - \sigma_{23}$, $\sigma_{12} - \sigma_{13}$, and $\sigma_{23} - \sigma_{22}$. These loads were applied such that they corresponded to the x and y components of the biaxial load represented as the radius of a circle as shown in Fig. 2, with θ varying from 0 to 180 deg. The two uniaxial loads required to generate the biaxial load state can be expressed as

$$\sigma_I = \sigma \cos\theta \quad \sigma_{II} = \sigma \sin\theta \quad (21)$$

where $\sigma = 10$ MPa was the resultant biaxial load vector magnitude, andσ_I andσ_{II} are the corresponding uniaxial loads. For this third study, the matrix modulus and fiber volume fraction were held constant at $0.01702 \times E_{11\text{fiber}}$ ($E_m = 4.0$ GPa) and 0.6, respectively.

Table 1 Baseline material properties of the fiber

Material	Type	E_1	E_2	G_{12}	ν_{12}	ν_{23}
AS4	Transversely isotropic	235 GPa	14 GPa	28 GPa	0.2	0.25

IV. Results and Discussion

As discussed previously, three series of simulations were carried out to quantify the dependencies of the interaction energy on material properties, fiber volume fraction, and loading conditions: 1) constant matrix and fiber modulus with varying fiber volume fraction, 2) varying matrix modulus for four different fiber volume fractions, and 3) constant material and microstructure properties with varying biaxial loading conditions.

A. Effect of Fiber Volume Fraction on Interaction Energy

Volume average quantities (stresses, strains, and stiffness) of the composite were extracted from the model, and then the total strain energy for the composite was calculated using Eq. (2). The volume average quantities (stresses, strains, and stiffness) of the constituents were also extracted. Constituent strain fluctuations and average stresses and strains were computed and used in Eqs. (19, 20) to give Φ_f and Φ_m. The total interaction energy was computed using

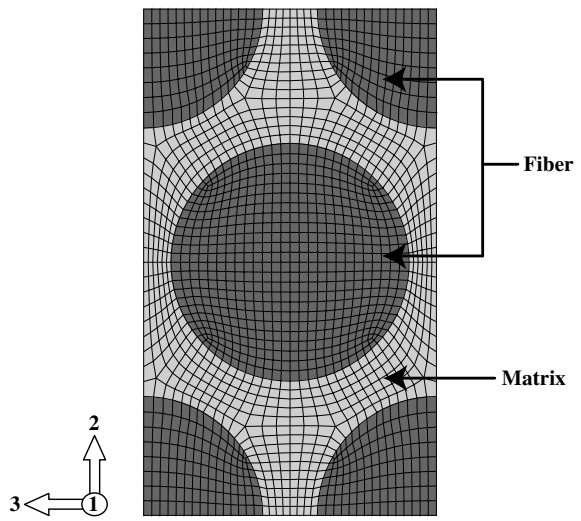

Fig. 1 RVE with hexagonal fiber packing for fiber volume fraction of 0.6.

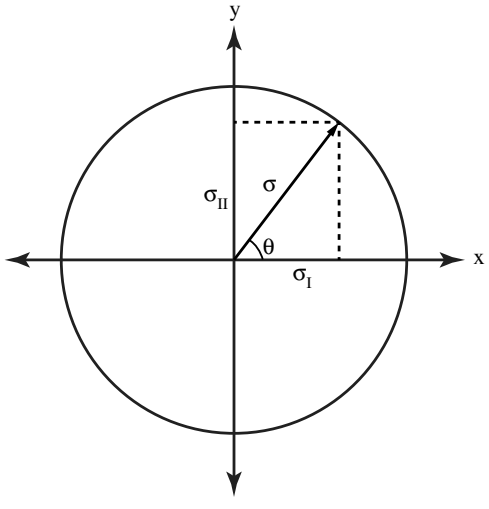

Fig. 2 Decomposition of biaxial load into its components.

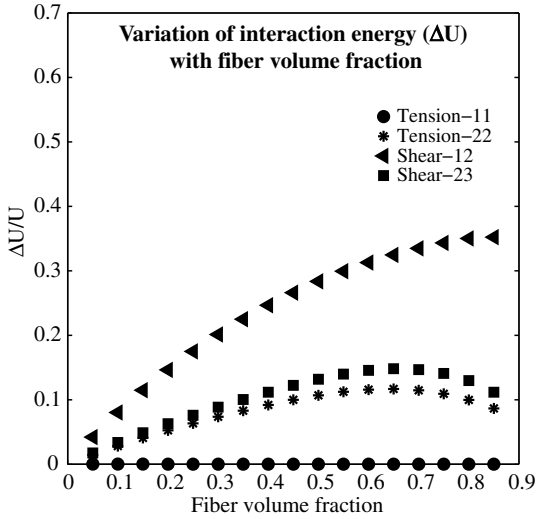

Fig. 3 Variation of interaction energy with fiber volume fraction.

Eq. (17). The interaction energy fraction ($\Delta U/U$) was computed for all the fiber volume fractions and each load case. The properties of the RVE were transversely isotropic; thus, only four (and not all six) load cases are unique.

Figure 3 shows $\Delta U/U$ as a function of fiber volume fraction for each load case. Three features of these data are of particular interest. First, the interaction energy is strongly dependent on the load case, and it can be a significant fraction of the total energy. It can be more than 30% of the total strain energy for longitudinal shear loading (shear-12), although it was negligible for unidirectional loading in the fiber direction (tension-11). Second, interaction energy increases with increasing volume fraction, up to typical volume fractions. Finally, transverse tension (tension-22) and transverse shear (shear-23) show a peak at a fiber volume fraction of about 0.65, very close to typical fiber volume fractions in aerospace-grade composites.

To qualitatively understand these features, consider stresses in an RVE with a fiber volume fraction of 0.6 subject to the four load cases. In case of longitudinal tension, shown in Fig. 4a, the stress distribution is uniform in each constituent throughout the structure; thus, strain fluctuations are minimal. Consequently, as shown in Eqs. (19) and (20), Φ_f and Φ_m, and correspondingly ΔU, are nearly zero for this load case. In the case of longitudinal shear, shown in Fig. 4b, the stress fluctuation is largest. Consequently, the interaction energy is maximized for this case, as seen in Fig. 3. This result is critically important because it means that, at a typical fiber volume fraction for aerospace-grade composites (60%), volume average constituent stresses neglect nearly 30% of the distortion energy in the composite in shear. The transverse tension and transverse shear load cases are shown in Figs. 4c and 4d, respectively. For both cases, the

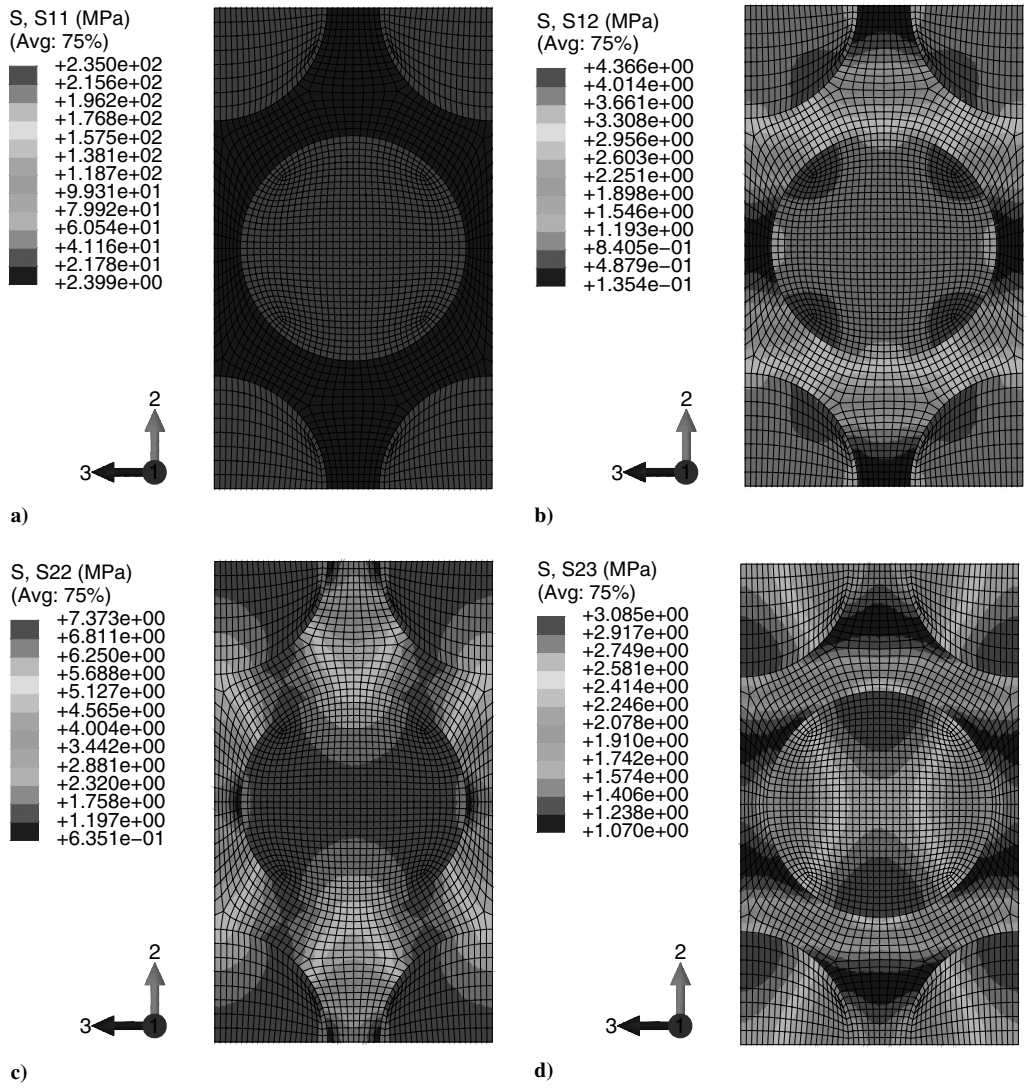

Fig. 4 Stress plots for a) load case tension-11, b) load case shear-12, c) load case tension-22, and d) load case shear-23.

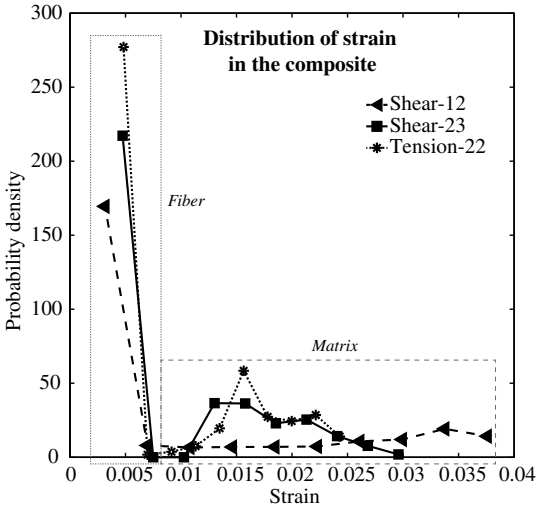

Fig. 5 Probability distribution function for strains for different load cases.

stress fluctuations are significant, and so interaction energy will not be negligible.

Stress distributions for longitudinal shear, transverse shear, and transverse tension are quantitatively shown in Fig. 5. The high probability densities at low strain values result from fiber strains; thus, the fluctuations in fiber strain are small. The matrix strain distribution consists of the larger strain values. The distinction is shown in Fig. 5 by enclosing fiber and matrix distribution in dashed lines. The matrix strain distribution is widest in longitudinal shear and smallest in transverse tension. Consequently, the interaction energy should be the least for transverse tension and the greatest for longitudinal shear, in agreement with Fig. 3.

An important observation to be made from these data is that the matrix strain distribution, and consequently the matrix strain fluctuation, is much broader and at much higher strains than the fiber strain distribution. This suggests that the small strain values of in fiber in conjunction with the even smaller strain fluctuations in fiber render the fiber a minor contributor to the interaction energy in the composite. To confirm this, the relative contribution of each constituent was examined. Figure 6 shows the relative matrix contribution to interaction energy plotted against fiber volume fraction for the four different load cases. The results are notable; up to typical fiber volume fractions, the matrix accounts for vast majority of interaction

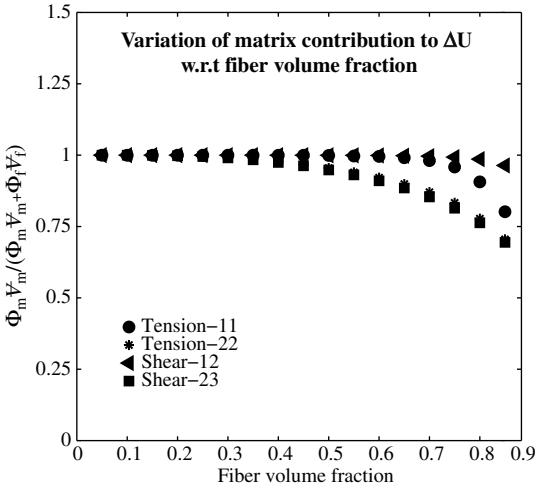

Fig. 6 Variation of contribution of matrix to interaction energy with fiber volume fraction.

energy. For a fiber volume fraction of 0.6, the matrix contributes almost the entirety (more than 99%) of the interaction energy of the composite for longitudinal shear loading, the most significant load case. Even for transverse tension and transverse shear, matrix contribution to interaction is about 90%. This result is important because it permits the interaction energy contribution of the fiber to be neglected, such that augmenting matrix failure theories with interaction energies can be the focus of future failure prediction efforts.

B. Effect of Relative Matrix Modulus on Interaction Energy

To investigate the variation of the interaction energy with matrix modulus, the matrix modulus was varied from 1 to 120% of the fiber-direction fiber modulus. Results were obtained for four fiber volume fractions: 0.05, 0.25, 0.60, and 0.85. Figure 7 shows the variation of relative interaction energy with matrix modulus for the four unique load cases. Figure 7a shows the variation of interaction energy with matrix modulus in longitudinal tension. For this load case, the interaction energy for all volume fractions is negligible. For the other three load cases, shown in Figs. 7b–7d, a general trend is observed; an initial increase in matrix modulus results in a decrease in interaction energy until a minimum is reached, after which additional increase in matrix modulus results in an increase in interaction energy. The minimum of the interaction energy occurs when the relevant fiber and matrix stiffnesses are the closest. For the load case in the transverse direction, shown in Fig. 7b, the interaction energy reaches a minimum when the matrix modulus is 5% of the fiber-direction fiber modulus, corresponding to a matrix modulus of 11.75 GPa, which is close to the fiber modulus in the transverse direction of 14 GPa. For a load case of longitudinal shear, shown in Fig. 7c, the interaction energy reaches a minimum when the matrix modulus is 30% of the fiber-direction fiber modulus, corresponding to a matrix shear modulus of 26.31 GPa, which is close to the fiber shear modulus in 12-direction of 28 GPa. For a load case of transverse shear, shown in Fig. 7d, the interaction energy reaches a minimum when the matrix modulus is 5% of the fiber-direction fiber modulus, corresponding to a matrix shear modulus of 4.38 GPa, which is close to the fiber shear modulus in 23-direction of 5.6 GPa. These results indicate that, for near isostress loadings, the interaction energy increases with increasing difference in the fiber and matrix modulus in the loading directions.

C. Effect of Combined Loading on Interaction Energy

In actual application, a composite is rarely subjected to uniaxial stresses, and so it is important to study the behavior of interaction energy under multi-axial load states. As discussed in Secs. IV.A and IV.B, the interaction energy for tensile loading in the longitudinal is negligible. Thus, it was not included in the study of combined loads. The fiber volume fraction and the matrix modulus were held constant at 0.6 and 4.0 GPa, respectively. The biaxial load is represented by the radius of a circle, as shown in Fig. 2, where θ is the angle made by the radius of the circle with the x axis, which is varied from 0 to 180 deg.

Figure 8 shows the variation of interaction energy under five types of biaxial loadings: $\sigma_{22} - \sigma_{33}$, $\sigma_{12} - \sigma_{22}$, $\sigma_{12} - \sigma_{23}$, $\sigma_{12} - \sigma_{13}$, and $\sigma_{23} - \sigma_{22}$. Under a biaxial longitudinal shear loading $\sigma_{12} - \sigma_{13}$, the interaction energy does not change, remaining constant at 27% of the total strain energy. This gives us an important metric for evaluating interaction energy under combined longitudinal shear loading. For a particular fiber-matrix combination and fiber volume fraction, interaction energy for biaxial longitudinal shear loading is always the same as that for pure longitudinal shear loading. Varying the ratio of σ_{12} to σ_{13} essentially rotates the stress distributions in the RVE but does not substantially change their relative quantitative values. When the RVE was subjected to a transverse normal $\sigma_{22} - \sigma_{33}$ biaxial loading, the interaction energy reached a minimum at 45 deg, corresponding to equal biaxial transverse loading. At this angle, a nearly uniform distribution of strains and stresses in the constituents is observed, similar to Fig. 4a, producing negligible interaction energy. In the remaining three cases ($\sigma_{12} - \sigma_{23}$, $\sigma_{12} - \sigma_{22}$, and

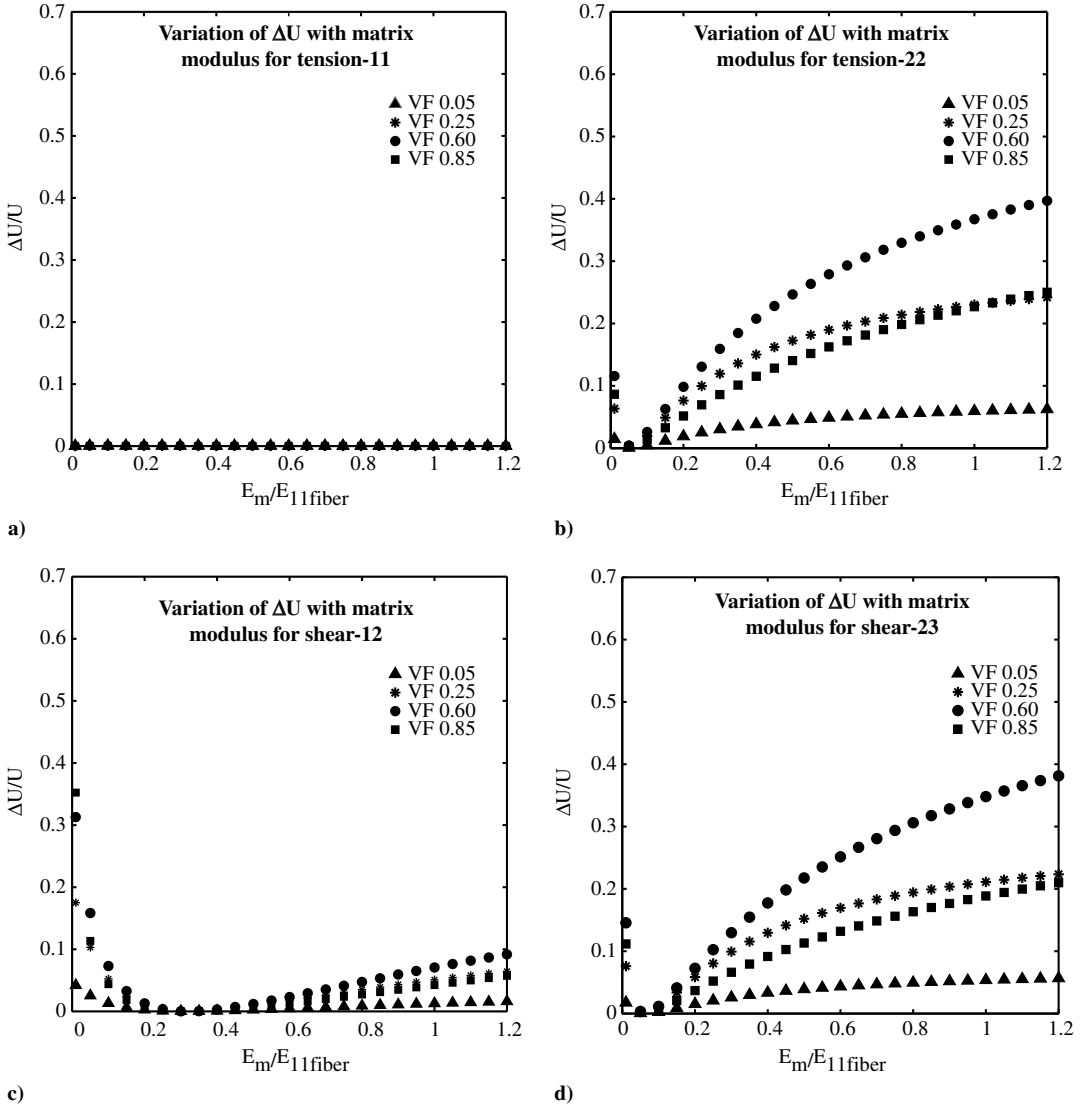

Fig. 7 Variations of interaction energy with matrix modulus in a) load case tension-11, b) load case tension-22, c) load case shear-12, and d) load case shear-23.

$\sigma_{23} - \sigma_{22}$), the maximum interaction energy occurs at 90 deg, which corresponds to a pure shear loading. This result is remarkable; any deviation from a pure shear loading reduces the interaction energy that would be computed. Thus, the composite shear loading in particular causes interaction energies to become significant, such that the interaction energy could be bounded by evaluating only a small number of load states.

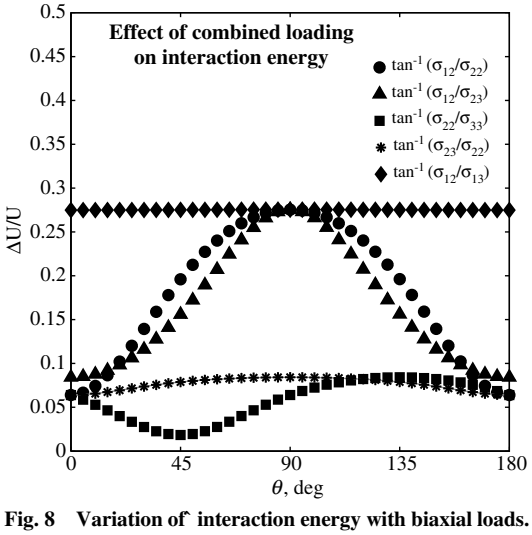

Fig. 8 Variation of` interaction energy with biaxial loads.

V. Conclusions

Accurate failure prediction is critical in efforts to maximize the promising advantages offered by composite materials. This requires physics-based failure prediction models, which necessarily require accurate understanding of constituent stress and strain. The use of volume average constituent stresses and strains to predict failure is a computationally efficient first step toward this effort but does not account for the entire strain energy in the composite. In this study, this missing energy, termed the interaction energy, was introduced, and expressions to define it were derived. A series of parametric finite-element studies were conducted to quantify the relative magnitude of the interaction energy for varying fiber volume fractions, matrix modulus, and loading conditions. Our results showed that, for typical carbon-epoxy composites used in the aerospace industry, the interaction energy may be as high as 30% of the total strain energy in the composite under shear loading, which is the load state yielding the highest relative interaction energy. Furthermore, for such systems, the matrix constituent is the major contributor to interaction energy. This result is important for future efforts to enhance composite failure prediction because it suggests that focus be placed on matrix failure criteria augmentation.

References

[1] Hinton, M. J., Kaddour, A. S., and Soden, P. D., "A Comparison of the Predictive Capabilities of Current Failure Theories for Composite Laminates, Judged Against Experimental Evidence," *Composites Science and Technology*, Vol. 62, Nos. 12–13, 2002, pp. 1725–1797. doi:10.1016/S0266-3538(02)00125-2

[2] Hinton, M. J., Kaddour, A. S., and Soden, P. D., "A Further Assessment of the Predictive Capabilities of Current Failure Theories for Composite Laminates: Comparison with Experimental Evidence," *Composites Science and Technology*, Vol. 64, Nos. 3–4, 2004, pp. 549–588. doi:10.1016/S0266-3538(03)00227-6

[3] Kaddour, A., and Hinton, M., "Maturity of 3D Failure Criteria for Fibre-Reinforced Composites: Comparison Between Theories and Experiments: Part B of WWFE-II," *Journal of Composite Materials*, Vol. 47, Nos. 6–7, 2013, pp. 925–966. doi:10.1177/0021998313478710

[4] Gotsis, P. K., Chamis, C. C., and Minnetyan, L., "Application of Progressive Fracture Analysis for Predicting Failure Envelopes and Stress–Strain Behaviors of Composite Laminates: A Comparison with Experimental Results," *Composites Science and Technology*, Vol. 62, Nos. 12–13, 2002, pp. 1545–1559. doi:10.1016/S0266-3538(02)00095-7

[5] Gotsis, P. K., Chamis, C. C., and Minnetyan, L. "Prediction of Composite Laminate Fracture: Micromechanics and Progressive Fracture," *Composites Science and Technology*, Vol. 58, No. 7, 1998, pp. 1137–1149. doi:10.1016/S0266-3538(97)00014-6

[6] Ha, S. K., Huang, Y., Han, H. H., and Jin, K. K., "Micromechanics of Failure for Ultimate Strength Predictions of Composite Laminates," *Journal of Composite Materials*, Vol. 44, No. 20, 2010, pp. 2347–2361. doi:10.1177/0021998310372464

[7] Huang, Y., Jin, C., and Ha, S. K., "Strength Prediction of Triaxially Loaded Composites Using a Progressive Damage Model Based on Micromechanics of Failure," *Journal of Composite Materials*, Vol. 47, Nos. 6–7, 2013, pp. 777–792. doi:10.1177/0021998312460261

[8] Mayes, J. S., and Hansen, A. C., "A Comparison of Multicontinuum Theory Based Failure Simulation with Experimental Results," *Composites Science and Technology*, Vol. 64, Nos. 3–4, 2004, pp. 517–527. doi:10.1016/S0266-3538(03)00221-5

[9] Hansen, A. C., Nelson, E. E., and Kenik, D. J., "A Comparison of Experimental Data with Multicontinuum Failure Simulations of Composite Laminates Subjected to Tri-Axial Stresses," *Journal of Composite Materials*, Vol. 47, Nos. 6–7, 2013, pp. 805–825. doi:10.1177/0021998313476394

[10] Garnich, M. R., and Hansen, A. C. "A Multicontinuum Theory for Thermal-Elastic Finite Element Analysis of Composite Materials," *Journal of Composite Materials* Vol. 31, No. 1, 1997, pp. 71–86. doi:10.1177/002199839703100105

[11] Huang, Z.-M., "A Bridging Model Prediction of the Ultimate Strength of Composite Laminates Subjected to Biaxial Loads," *Composites Science and Technology*, Vol. 64, Nos. 3–4, 2004, pp. 395–448. doi:10.1016/S0266-3538(03)00220-3

[12] Huang, Z.-M., "Correlation of the Bridging Model Predictions of the Biaxial Failure Strengths of Fibrous Laminates with Experiments," *Composites Science and Technology*, Vol. 64, Nos. 3–4, 2004, pp. 529–548. doi:10.1016/S0266-3538(03)00222-7

[13] Huang, Z.-M., and Zhou, Y.-X., "Correlation of the Bridging Model Predictions for Triaxial Failure Strengths of Composites with Experiments," *Journal of Composite Materials*, Vol. 47, Nos. 6–7, 2013, pp. 697–731. doi:10.1177/0021998312453864

[14] Paley, M., and Aboudi, J., "Micromechanical Analysis of Composites by the Generalized Cells Model," *Mechanics of Materials*, Vol. 14, No. 2, 1992, pp. 127–139. doi:10.1016/0167-6636(92)90010-B

[15] Bednarcyk, B. A., and Arnold, S. M., "Micromechanics-Based Modeling of Woven Polymer Matrix Composites," *AIAA Journal*, Vol. 41, No. 9, 2003, pp. 1788–1796. doi:10.2514/2.7297

[16] Moncada, A. M., Chattopadhyay, A., Bednarcyk, B. A., and Arnold, S. M., "Micromechanics-Based Progressive Failure Analysis of Composite Laminates Using Different Constituent Failure Theories," *Journal of Reinforced Plastics and Composites*, Vol. 31, No. 21, 2012, pp. 1467–1487. doi:10.1177/0731684412456330

[17] Pineda, E. J., Waas, A. M., Bednarcyk, B. A., Collier, C. S., and Yarrington, P. W., "Progressive Damage and Failure Modeling in Notched Laminated Fiber Reinforced Composites," *International Journal of Fracture*, Vol. 158, No. 2, 2009, pp. 125–143. doi:10.1007/s10704-009-9370-3

[18] Moncada, A. M., Reynolds, W. D., Chattopadhyay, A., Bednarcyk, B. A., and Arnold, S. M., "An Explicit Multiscale Model for Progressive Failure of Composite Structures," *50th AIAA/ASME/ASCE/AHS/ASC Structures, Structural Dynamics, and Materials Conference*, AIAA Paper 2009-2549, May 2009.

[19] Bednarcyk, B. A., Aboudi, J., and Arnold, S. M., "Micromechanics Modeling of Composites Subjected to Multiaxial Progressive Damage in the Constituents," *AIAA Journal*, Vol. 48, No. 7, 2010, pp. 1367–1378. doi:10.2514/1.45671

[20] Pineda, E. J., Bednarcyk, B. A., Arnold, S. M., and Waas, A. M., "On Multiscale Modeling: Preserving Energy Dissipation Across the Scales with Consistent Handshaking Methods," *54th AIAA/ASME/ASCE/AHS/ASC Structures, Structural Dynamics, and Materials Conference*, AIAA Paper 2013-1474, 2013.

[21] Gosse, J. H., and Christensen, S. "Strain Invariant Failure Criteria for Polymers in Composite Materials," *19th AIAA Applied Aerodynamics Conference*, AIAA Paper 2001-1184, April 2001.

[22] Tay, T. E., Tan, S. H. N., Tan, V. B. C., and Gosse, J. H., "Damage Progression by the Element-Failure Method (EFM) and Strain Invariant Failure Theory (SIFT)," *Composites Science and Technology*, Vol. 65, No. 6, 2005, pp. 935–944. doi:10.1016/j.compscitech.2004.10.022

[23] "Materials Genome Initiative for Global Competitiveness," Executive Office of the President: National Science and Technology Council, Washington, D.C., 2011, p. 19.

[24] *Integrated Computational Materials Engineering: A Transformational Discipline for Improved Competitiveness and National Security*, National Academies Press, Washington, D.C., 2008, p. 152.

[25] Hashin, Z., "Analysis of Composite Materials—A Survey," *Journal of Applied Mechanics*, Vol. 50, No. 3, 1983, pp. 481–505. doi:10.1115/1.3167081

[26] Sun, C. T., and Vaidya, R. S., "Prediction of Composite Properties from a Representative Volume Element," *Composites Science and Technology*, Vol. 56, No. 2, 1996, pp. 171–179. doi:10.1016/0266-3538(95)00141-7

[27] Hill, R., "Elastic Properties of Reinforced Solids: Some Theoretical Principles," *Journal of the Mechanics and Physics of Solids*, Vol. 11, No. 5, 1963, pp. 357–372. doi:10.1016/0022-5096(63)90036-X

[28] Teply, J. L., and Dvorak, G. J., "Bounds on Overall Instantaneous Properties of Elastic-Plastic Composites," *Journal of the Mechanics and Physics of Solids*, Vol. 36, No. 1, 1988, pp. 29–58. doi:10.1016/0022-5096(88)90019-1

[29] Abaqus, Software Package, Ver. 6.11, Dassault Systèmes, Vélizy-Villacoublay, France, 2011.

P. Weaver
Associate Editor